Journal of Inorganic and General Chemistry
ZAAC
Zeitschrift für anorganische und allgemeine Chemie
www.zaac.wiley-vch.de
RESEARCH ARTICLE

DOI: 10.1002/zaac.202300166

Special Collection

Synthesis, Structure and Physical Properties of the Sodium-Rich Phosphidogermanate Na_8GeP_4

Manuel Botta,[a] Sabine Zeitz,[a] and Thomas F. Fässler*[a]

Dedicated to Prof. Dr. Michael Ruck on the occasion of his 60th birthday.

Sodium ion conductor materials hold promise to be an affordable substitute for ever growing lithium demand. To achieve high ionic conductivity in all-solid state ion conductor materials, fundamental understanding of the atomic structure of the materials as well as the structure-property relationship are basic prerequisites. It has been recently shown that phosphide-based materials such as the superionic conductor Li_9AlP_4 or the lithium-rich $Li_{14}SnP_6$ show great ionic conductivities what makes them promising candidates for solid electrolyte materials. Here, we present the investigation of the sodium rich phase Na_8GeP_4 that reveals a similar structure if compared to the lithiated phases. Na_8GeP_4 is synthesized via a ball-milling procedure and a subsequent annealing process. Crystallographic investigation by Rietveld method shows that Na_8GeP_4 crystallizes in the cubic space group $Fd\bar{3}m$ (no. 227) with a cell parameter of a = 13.4230 Å at 298 K. While it shares many structural motifs of Li_8GeP_4, it is not isotypic but crystallizes in the Na_8SnSb_4 structure type. Impedance spectroscopy as well as density functional theory calculations reveal that Na_8GeP_4 is a good electronic conductor with a band gap of 1.9 eV.

Introduction

All solid-state lithium ion batteries hold promise to conquer rising demand on high density energy storage materials while at the same time reduce safety risks.[1] While there is a rapidly increasing interest in the evolution of such battery systems for various applications the, number of publications dealing with alternatives aside from Li^+ as the conducting ion is surprisingly low. Sodium solid electrolyte materials are considered an effective alternative for lithium and show great potential, especially for stationary applications with the high abundance of sodium resulting in far better affordability.[2] Thus, it is needed to investigate material classes to provide sodium containing solid electrolytes that can match the performance of their lithium counterparts.[3] Criteria for archiving a high ionic conductivity in a crystalline solid are firstly a high charge carrier density as well as a number of available lattice sites to provide the means for fast ionic motion. Secondly, the electrolyte requires a low activation energy for the mobility of the ion charge carrier as it can be found in structures where the cation sites are located in face-sharing polyhedra formed by anions. Lastly, a low electronic conductivity is needed to prevent electronic leakage leading to reduced efficiency of the battery.[4] These attributes can be found in phosphate materials like the NASICON family[5] or in sulfide based materials like Na_3PS_4[6] which already achieves an ionic conductivity of up to 0.46 mS/cm^{-1}. Optimization attempts on these materials have led to the finding of compounds like $Na_{11}Sn_2PS_{12}$[7] where the ionic conductivity can reach up to 3.7 mS/cm^{-1}.

The compound classes of lithium phosphidotrielates and tetrelates also provide materials that exhibit these attributes and since they possess similar but different structures, the influence of atomic structure on the lithium ion mobility can be studied. Supertetrahedral structures like L_2SiP_2 or $LiSi_2P_3$[8,9a] exhibit moderate low activation energies for ionic motion, a prerequisite for good ionic conductivity. Compounds such as the polymorphs of Li_8TtP_4 (*Tt* = Si, Ge, Sn)[9] comprise of discrete $[TtP_4]^{8-}$ tetrahedra which in turn lead to very high concentrations of alkali cations and a good ionic conductivity. The latter structures are closely related to the antifluoride type CaF_2 comprising a cubic close packing (*ccp*) of phosphorous atoms that creates eight tetrahedral and four octahedral voids per formula unit with four P atoms. As only nine of these twelve voids are filled (one with a covalently bound tetrel element and eight with lithium atoms), the remaining vacancies allow for ionic motion in the system. Since tetrahedral and octahedral voids share faces in a simplistic view, the window for diffusion pathways is greater compared to cases in which only edge-sharing polyhedral are present. Further investigation led to the finding of $Li_{14}TtP_6$ (*Tt* = Si, Ge, Sn)[10] that exhibit the so far

[a] M. Botta, S. Zeitz, Prof. Dr. T. F. Fässler
Chair of Inorganic Chemistry with Focus on New Materials, TUM School of Natural Sciences
Technische Universität München, Lichtenbergstraße 4, D-85747 Garching, Germany
E-mail: Thomas.faessler@lrz.tum.de

Supporting information for this article is available on the WWW under https://doi.org/10.1002/zaac.202300166

Special Collection *This article is part of a Special Collection dedicated to Professor Michael Ruck on the occasion of his 60th birthday. Please see our homepage for more articles in the collection.*

highest lithium content in this class of materials. The formal addition of two units Li_3P to Li_8TtP_4 ($2\ Li_3P + Li_8TtP_4 = Li_{14}TtP_6$) arises in a complete disorder of Li and tetrel atoms in the tetrahedral position. In addition, the aliovalent substitution of the tetrel elements with triel elements to was investigated. The increase of the numbers of charge carriers in Li_9TrP_4 (Tt = Al, Ga, In),[11] which also exhibit structures of comprise discrete $[TrP_4]^{9-}$ tetrahedra, result in very similar crystals structures as the phosphido-tetrelates and exhibit the so far highest ionic conductivities of up to 4.5 mS/cm^{-1} at room temperature for Li_9GaP_4.

These findings led us to the investigation whether the structural principles and related properties of phases with discrete tetrahedra could be transferred to the heavier homologue Na. For compounds with supertetrahedral phosphidosilicates comprising SiP_4 tetrahedra fast ionic conductivity has been reported for heavier alkali metals Na und K.[12] The class of sodium phosphidogermanates has been shown to exhibit a great structural variety with compounds that crystallize in different kinds of polyanionic frameworks resulting in two or three-dimensional infinitely connected structures such as $NaGe_3P_3$, $Na_2Ge_3P_3$ and $Na_5Ge_7P_5$ comprising heteroatomic Ge–P polyanions mimicking the structure of fibrous red phosphorus.[13] The Ge–P frameworks share the motif of connected tetrahedral units, where at least two tetrahedra share P atoms and the degree of connectivity is determined by the amount of sodium atoms per formula unit.

We report on the synthesis and characterization of the compound Na_8GeP_4 where we achieved to synthesize a sodium phosphidogermanate with isolated $[GeP_4]^{8-}$ building units by using a synthesis protocol involving mechanical alloying and subsequent annealing. The compound is characterized via X-ray diffraction, the crystal structure was solved using the Rietveld method. Thermal properties of the sample were analyzed using differential scanning calorimetry and the electronical structure of the material was investigated by electrochemical impedance spectroscopy and density functional theory calculations.

Experimental Section

All steps of synthesis and sample preparation were carried out inside an argon-filled glove box (MBraun, $p(H_2O)$, $p(O_2) < 0{,}1$ ppm) or in under Ar atmosphere and vacuum ($< 2\times10^{-2}$ mbar) sealed containers. Prior to use, sodium (Na, rods, Merck–Schuchardt, >99%) was cleaned from oxide layers. Germanium (EVOCHEM GmbH, 99,999%) Phosphorus (P, red, powder, Sigma–Aldrich, 97 %) were used without any further purification. All obtained compounds are sensitive to oxygen and moisture with the latter showing vigorous reaction that results in flammable and toxic gases. Therefore, the disposal must be addressed under proper ventilation and in small amounts at a time.

Synthesis of Na_8GeP_4

Na_8GeP_4 was synthesized in a two-step synthesis from the elements via ball milling and subsequent annealing (XRD in the supporting information). To achieve higher phase purity, an excess of phosphorus resulting in the stoichiometry "$Na_8GeP_{4.2}$" was used. Sodium pieces (1427.1 mg, 62.07 mmol, 8.0 equiv.), germanium powder (563.6 mg, 7.75 mmol, 1.0 equiv.) and red phosphorus (1040.6 mg, 33.59 mmol, 4.2 equiv.) were treated in a ball mill (Retch PM 100 planetary mill) for 18 hours at 350 rpm in intervals of 10 min with direction reversal and subsequent 5 min resting using a WC milling set (50 mL jar with 3 balls with a diameter of 15 mm each). The obtained black mixed powder was pressed into pellets of 8 mm diameter and sealed in silica glass ampules in batches of 200 mg. The tubes were heated with 4 K min^{-1} to 633 K and dwelled for 40 h in a muffle furnace (Nabertherm, L5/11/P330) and cooled down at a rate of 1 K min^{-1}. After grinding, a black powder was obtained. The product contains $Na_{10}Ge_2P_6$ according to PXRD measurements.

Synthesis of $Na_{10}Ge_2P_6$

$Na_{10}Ge_2P_6$ that has been described before[14] was synthesized in analogy by a two-step synthesis from the elements via ball milling and subsequent annealing. Sodium (1024.5 mg, 44.6 mmol, 5.0 equiv.), germanium (647.3 mg, 8.91 mmol, 1.0 equiv.) and red phosphorus (853.8 mg, 27.56 mmol, 3 equiv.) were treated in a ball mill applying the same procedure as described above. The obtained black mixed powder was sealed into niobium crucibles in batches of 200 mg using an arc furnace (Edmund Bühler MAM1). The sealed ampules were enclosed in evacuated silica reaction containers. The containers were heated in a tube furnace (HTM Reetz Loba) with 4 K min^{-1} up to 873 K, dwelled for 12 h and cooled down at a rate of 2 K min^{-1}. After grinding, a black powder was obtained.

Powder X-ray diffraction

For powder X-ray diffraction (PXRD) measurements, the samples were ground in an agate mortar and sealed inside 0.3 mm glass capillaries. PXRD measurements were performed at room temperature on a STOE Stadi P diffractometer (Ge(111) monochromator, Cu $K\alpha_1$ radiation, $\lambda = 1.54056$ Å) with a Dectris MYTHEN 1 K detector in Debye–Scherrer geometry. The raw powder data were processed with the software package WinXPOW.[15]

Rietveld refinement

Rietveld refinements of Na_8GeP_4 were executed using the full profile Rietveld method within the FullProf program package.[16] The structure of Na_8SnSb_4 by Eisenmann et al. was used as structural model.[25] The Thomson-Cox-Hermann functional was used to model the peak profile shape. Background contribution was determined using a linear interpolation between selected data points in non-overlapping regions. Scale factor, zero angular shift, profile shape parameters, resolution (Caglioti) parameters, asymmetry and lattice parameters as well as fractional coordinates of atoms and their displacement parameters were refined freely. Further details of the crystal structure investigation may be obtained from the Cambridge Crystallographic Data Centre, CCDC, 12 Union Road, Cambridge CB21EZ, UK (Fax: +44-1223-336-033; E-mail: deposit@ccdc.cam.ac.uk) on quoting the depository number CSD-2279391.

Differential scanning calorimetry (DSC)

For thermal analysis, samples were sealed in a niobium ampoule and measured on a DSC machine (Netzsch, DSC 404 Pegasus) under a constant gas flow of 75 mL min^{-1}. The sample was heated to 973 K and cooled to 473 K twice at a rate of 5 K min^{-1}. To determine the onset temperatures of the DSC signals, the PROTEUS Thermal

Analysis software was used[18] and visualization was realized using OriginPro 2021.

Raman-Spectroscopy

Raman spectra were measured using an inVia Raman microscope (Renishaw, RE04), equipped with a CCD detector. The powdered sample was sealed into a 0.3 mm glass capillary and irradiated with a 785 nm laser beam for 1 s at 0.1 % laser power using a microscope equipped with a 50-fold magnifying objective and a grating with 1800 lines mm^{-1}. For the final spectrum, 100 single measurements were averaged. The software WiRe 4.2[19] (build 5037, Renishaw 2002) was used for data recording.

Electronic Structure Calculations

The computational analysis of Na_8GeP_4 was performed using the Crystal17 program package and hybrid density functional methods.[20] A hybrid exchange correlation functional after Perdew, Burke and Ernzerhof (PBE0),[21] and triple-zeta valence + polarization level basis sets for Na, Ge and P derived from the Karlsruhe basis sets were applied (further details are in the Supporting Information).[22] The starting geometry was taken from the experimental data, and the structure was fully optimized within the constraints imposed by the space group symmetry. Band structure and density of states (DOS) were calculated. The Brillouin Zone path of Na_8GeP_4, Γ–X–U | K–Γ–L–W–X was provided by the web application *SeeK-path*.[23] The nature of a stationary point on the potential energy surface was confirmed to be a minimum by a frequency calculation at Γ-point. No imaginary frequencies were observed. Using the results of the frequency calculation, a theoretical Raman spectrum was calculated by utilizing a analytical CPHF/CPKS scheme (coupled perturbed Hartree Fock/Kohn Sham). The full width at half maximum (FWHM) was set to 8 cm^{-1}, the pseudo-Voigt broadening to 50:50 Gaussian:Laurenzian and the laser wavelength to 785 nm. To assign signals in the spectrum to vibrations of the lattice, the software Jmol 14.14.1[24] was used for visualizing of theoretical vibration modes.

Impedance spectroscopy and DC conductivity measurements

The electrochemical impedance spectroscopy for Na_8GeP_4 was performed in an in-house designed cell. The detailed setup and procedure have been described by us before.[10a] Powdered samples of Na_8GeP_4 (330 mg) were placed between two 8 mm dies, and the screws were fastened with a torque of 30 Nm, compressing the sample to ca. 72 % of the theoretical density. Impedance spectra were recorded on a Biologic potentiostat (VMP-300) in a frequency range from 7 MHz to 100 mHz at a potentiostatic excitation of 10 mV. Data was treated using the software EC-Lab (V 11.36). The measurements were performed in an Ar-filled glove box at 299 K. The electronic conductivity was determined with the same setup using a potentiostatic polarization procedure, applying voltages of 50, 100 and 150 mV for 7 h each.

Results

Synthesis and structure of Na_8GeP_4

During our search for new materials in the class of sodium phosphidogermanates we managed to synthesize and resolve the compound Na_8GeP_4 which crystallizes in the Na_8SnSb_4 structure type[25] and marks the first compound with this 8/1/4 stoichiometry in the system of sodium phoshidotetrelates to the best of our knowledge. The compound can be obtained in gram scale from the elements via a two-step synthesis procedure. A reactive mixture of elemental sodium, germanium and red phosphorous with the formal stoichiometry "$Na_8GeP_{4.2}$" is received via ball milling procedure and subsequent annealing. Obtaining a phase pure sample has proven critical since slow decomposition of Na_8GeP_4 into $Na_{10}Ge_2P_6$ and Na_3P ($2\ Na_8GeP_4 = Na_{10}Ge_2P_6 + 2\ Na_3P$) starts occurring at roughly 350 °C. DSC measurements (Figure S8 in the supporting information) do not show signals that can be attributed to a reversible reaction but instead reveal, that an irreversible decomposition of a previously annealed sample occurs at around 460 °C. Samples annealed at 420 °C already exhibit $Na_{10}Ge_2P_6$[14] as main product in the XRD pattern (Figure S2), so it is likely that the decomposition starts at even lower temperatures. However, only incomplete reaction is observed at this temperature with longer annealing times not leading to better results. Taking all this into account the highest purity was obtained with the above given procedure.

According to Rietveld analysis of the powder XRD data shown in Figure 1a a ratio of 82(1) wt.% of Na_8GeP_4 and 18(1) wt.% of $Na_{10}Ge_2P_6$ has been achieved. Atomic coordinates and isotropic displacement parameters are given in Table 1.Rietveld refinement data is given in Table 2. Interatomic distances and angles of Na_8GeP_4 are given in the Supporting Information (Table S1).

Na_8GeP_4 crystallizes in the space group $Fd\bar{3}m$ (no. 227) with a lattice parameter of a = 13,4230 Å at 298 K. Comparison of the data with compounds having the same stoichiometry with the lighter alkali homologue lithium instead of Na (Li_8TtP_4 (Tt = Si, Ge, Sn))[9b,c] show that Na_8GeP_4 is not isotypic. Thus, Na_8GeP_4 represents the first compound in the system of alkali-metal phosphide-tetrelates that adapts this structure type. Structure determination was performed by Rietveld analysis based on powder X-ray diffraction using the structure of Na_8SnSb_4 as a start model.[25] The structure contains one Ge-position, one fully occupied P-position and two crystallographic independent Na positions (Ge1, P1, Na1 and Na2). Like the lithium compounds, it is closely related to the antifluoride structure type (or Li_3Bi-

Table 1. Atomic coordinates and isotropic displacement parameters for Na_8GeP_4 from Rietveld analysis.

Atom	Wyck.	*x/a*	*y/b*	*z/c*	U_{iso} [Å^2]
P1	32e	0.22852(6)	0.22852(6)	0.22852(6)	0.0137(5)
Ge1	8a	1/8	1/8	1/8	0.0170(5)
Na1	16c	0	0	0	0.028(1)
Na2	48f	0.4005(1)	1/8	1/8	0.0279(6)

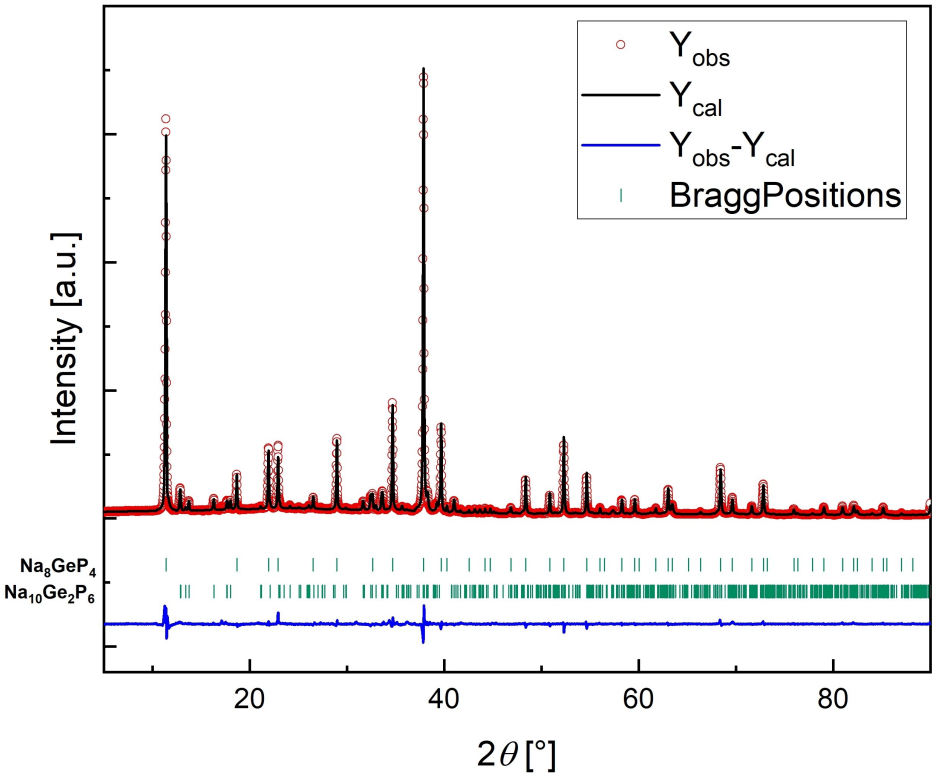

Figure 1. Rietveld refinement of the powder X-Ray pattern of Na_8GeP_4. The red line indicates observed intensities, the black line the calculated intensities and the blue line shows the difference. Bragg positions are depicted as green dashes. The Na_8GeP_4:$Na_{10}Ge_2P_6$ ratio is 81,3(4) wt.%: 18,6(2) wt.%.

Table 2. Rietveld refinement data of powder x-Ray diffraction on Na_8GeP_4 at 293 K.

Empirical Formula	Na_8GeP_4
T/K	293
formula weight/g mol^{-1}	380.4
space group (no)	$Fd\bar{3}m$ (227)
unit cell parameters/Å	$a = 13.4230(2)$
Z	8
V/Å^3	2418.53 (5)
ρcalc./g cm^{-3}	2.08943
θ range/deg	5–90.3
Rp	4.67
Rwp	6.27
Rexp	3.57
X^2	3.09
R_{Bragg}	3.4
R_f	2.38

type) with P atoms on Ca positions forming a cubic closed atom packing and Ge and Li atoms on F positions filling the tetrahedral voids. In the present compound the P atoms form a slightly distorted *ccp* lattice. Space group symmetry allows for three different Wyckoff positions centering the tetrahedral voids, namely 8a, 8b and one 48f position. The 8a as well as the 48f position are fully occupied by Ge and Na, respectively, while the 8b Position remains vacant. The remaining sodium atoms are located at a fully occupied 16c position, which centers an octahedral void in the *ccp* of P atoms. In this way isolated highly charged $[GeP_4]^{8-}$ tetrahedra are formed, which are surrounded by eight Na^+ per formula unit. In summary, 87.5% of the tetrahedral and 50% of the octahedral voids are occupied by Ge and Na atoms in an ordered manner. The Ge–P bond length of 2.4068(8) Å is within the characteristic range of Ge–P interactions such as in related compounds like $Na_{10}Ge_2P_6$ (2.334(1)–2.425(1) Å).[14] With respect to the CaF_2 unit cell, the present structure represents a 2×2×2 superstructure based on the *ccp* of P atoms, just as for Li_8TtP_4 (Tt = Si, Ge, Sn).[9b,c] The arrangement of the Ge atoms (or GeP_4 tetrahedra) can be rationalized within the unit cell in a hierarchical view as a bicapped hexagon in chair conformation (Figure 2b). The distortion of the *ccp* lattice comes in form of a shift of the P-atoms towards the Ge position leaving the $[GeP_4]^{8-}$ tetrahedra perfectly T_d-symmetric with an P–Ge–P angle of 109.47°. On the contrary, the tetrahedra around the Na2 position are heavily distorted wherein the central atom is shifted towards a triangular plane. This shift can be explained structurally as the neighboring octahedral void sharing this triangular plane are not occupied. A visual representation of the polyhedral network as well as each single polyhedron is given in the Supporting Information (Figure S4, S5). The occupation parameters of sodium atoms were first refined without restrictions and resulted in site occupancy factors (S.O.F) of 0.989 for Na1 and 0.987 for Na2 hinting for a full occupation within the standard

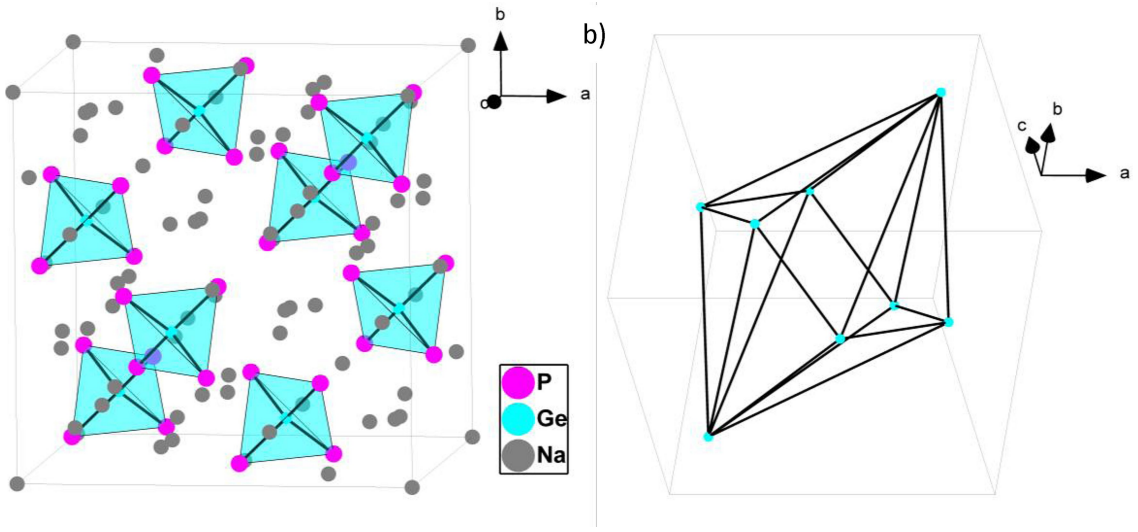

Figure 2. a) The crystal structure of Na_8GeP_4. Sodium is located surrounding the GeP_4 tetrahedra in tetrahedral and octahedral voids of the phosphorous ccp lattice. b) Arrangement of Ge atoms as a hexagonal bipyramidal structure with a tilted graphite-like basis. The Na, Ge and P atoms are drawn in grey, blue and pink respectively. The GeP_4^{8-} tetrahedra are highlighted in turquoise. The displacement ellipsoids are shown at a 90% probability level.

deviation. Hence, the occupancy was set to 1 in the final refinement steps. An electron precise valence compound Na_8GeP_4 is reached when both sodium positions are fully occupied.

To further investigate and confirm the structure, Raman measurements were conducted on a sample of Na_8GeP_4. Since the sample contains $Na_{10}Ge_2P_6$ as an impurity, phase pure $Na_{10}Ge_2P_6$ was measured for comparison as well. For both compounds theoretical Raman spectra were calculated. All data are shown in Figure 3. $Na_{10}Ge_2P_6$ shows Raman signals with high intensity predominantly in the range of 300–350 cm^{-1} which matches nicely with the expected spectrum (pink and yellow spectra, respectively). The intense signals can be attributed to asymmetric Ge–P stretching vibrations that fit to the characteristic dimeric building unit found in this compound.[14]

The calculated spectrum of Na_8GeP_4 exhibits one characteristic signal at 152 cm^{-1} which originates from symmetrical Na–Ge stretching vibrations and which is observed in the measured spectrum as well (Figure 3, red and blue spectra, respectively). As expected; the measured spectrum shows both characteristic signal groups of both compounds.

Group-Subgroup relationship

As the substitution of lithium with the heavier homologue sodium leads to an ordering of Ge atoms that is not isotypical to either one of the two polymorphs existing for the lithium analogous compounds, the question arises how the symmetry of the new polymorph is connected to the others. Therefore, we applied the Bärnighausen method to determine the group-subgroup relationship via a crystallographic tree. The crystal structure shows the same isolated $[GeP_4]^{8-}$ tetrahedral building units like the lithiated compounds and crystallizes in a cubic structure as well. The lattice parameter is larger due to substitution of lithium by sodium but fits the cell expansion observed when comparing binary lithium and sodium phosphides Li_3P and Na_3P.[26] All polymorphs can be connected to the antifluoride CaF_2 aristotype and form a slightly distorted *ccp* of P-atoms. Additionally in all the polymorphs the tetrahedral voids are occupied with alkali-metal ions and Ge atoms in an ordered manner while the octahedral voids are partially filled with alkali ions to balance the charge. The relationship of the cubic space groups of the α-Li_8GeP_4 polymorph $Pa\bar{3}$ and the β-Li_8GeP_4 polymorph $P\bar{4}3n$ has been investigated in a previous work[9b] and shows that these are surprisingly not related via a direct group-subgroup relation but instead via the space group of the aristotype CaF_2 $Fm\bar{3}m$.

The space group of the Na_8GeP_4 polymorph $Fd\bar{3}m$ exhibits the same behavior as it is not directly related to any of the two polymorphs of the lithiated compounds α- and β-Li_8GeP_4 but shares the same aristotype CaF_2 (Figure 4, symmetry degradation corresponding to Bärnighausen is given in the Supporting information S11). Thus, the conversion of the present compound into another polymorph is most likely kinetically hindered as described in the previous work. The transformation might occur at higher temperatures, however rapid decomposition of Na_8GeP_4 at elevated temperature was observed during our synthesis protocol. This emphasizes again that a different synthesis route is needed to further investigate the compound Na_8GeP_4.

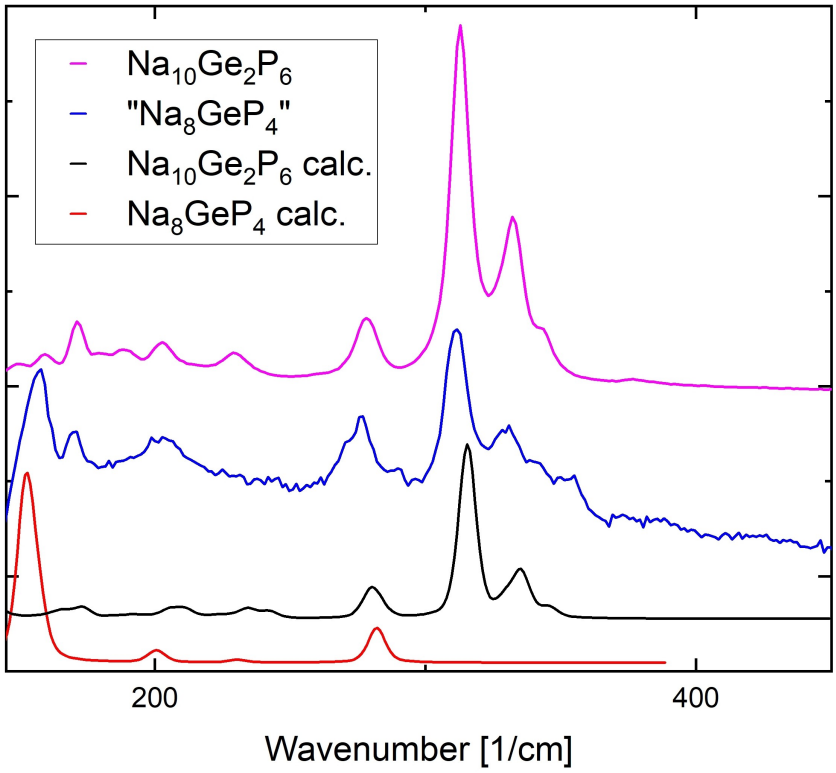

Figure 3. Measured Raman spectra of the product "Na_8GeP_4" and phase pure $Na_{10}Ge_2P_6$ depicted in blue and magenta, respectively. Additionally depicted are the calculated Raman spectra of Na_8GeP_4 and $Na_{10}Ge_2P_6$ in red and black, respectively. Intensities are scaled to ensure readability, as they differed gravely between the two measured samples.

Investigation of the electronic properties of Na_8GeP_4

Electrochemical impedance spectroscopy was performed in order to investigate the ionic conductivity of Na_8GeP_4. Since no phase pure sample of Na_8GeP_4 could be prepared and only a mixture with roughly 18 mass% impurity of $Na_{10}Ge_2P_6$ could be measured, only qualitative analysis can be performed on the impedance data. The impedance spectra at different temperatures are displayed in the Supporting Information (Figure S10). The measurement was performed in a blocking electrode configuration. The spectra feature partially the high-frequency semicircles however due to the very low resistance the front part was at the limit of the measurement setup. The semicircles were fitted by a parallel circuit of a resistor and a constant phase element (R/Q) in which R represents contribution of both electric and ionic conductivity of the sample. The constant phase element could be fitted to α-values of $\approx$0.87 and had a capacitance of $\approx 4\times10^{-9}$ F. The conductivity obtained from the PEIS measurement was determined to be $\sigma(Na_8GeP_4) = 9.57\times10^{-3}$ S cm^{-1}. Additionally, DC polarization measurements were performed to investigate the electronic conductivity of the compound. Measurements in the range of 50 to 150 mV reveal an electronic conductivity of 3.29×10^{-3} S cm^{-1} at 298 K. As the conductivity value obtained by DC polarization is in close range to the value obtained by the PEIS measurement, the Nyquist plot can be interpreted as showing only the electronic conductivity and no semicircle for the ionic conductivity can be measured.

The side product $Na_{10}Ge_2P_6$ was not characterized via electrochemical methods up to date. Hence, we developed a protocol (see experimental for details) to synthesize a phase pure sample and performed PEIS and DC measurements. The impedance spectra measured at different temperatures are given in the Supporting information (Figure S10). The spectra feature a high-frequency semicircle but no low frequency tail. The semicircles were again fitted by a parallel circuit of a resistor and a constant phase element (R/Q) in which R represents contribution of both electric and ionic conductivity of the sample. For the constant phase element, the fit of the data acquired at 298 K resulted in α-values of $\approx$0.96 and capacitance of $\approx 0{,}7\times10^{-9}$ F. The ionic conductivity determined by the PEIS is $\sigma(Na_8GeP_4) = 1.94\times10^{-5}$ S cm^{-1}. DC polarization was performed equivalent to Na_8GeP_4 and revealed an electronic conductivity of 1.27×10^{-5} S cm^{-1} at 298 K. Hence, the first semicircle of the Nyquist plot of $Na_{10}Ge_2P_6$ represents electronic conductivity. A second very small semicircle could be interpreted into the tail of the first one but the resolution of the measurement did not allow for a more concrete interpretation. Thus, we determined $Na_{10}Ge_2P_6$ as a pure electronic conductor.

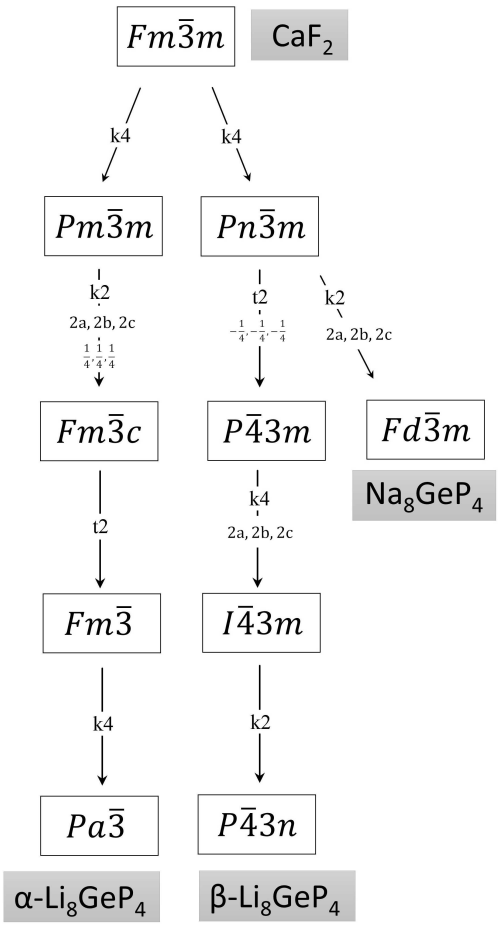

Figure 4. Bärnighausen tree of Group-subgroup relationship between CaF_2 and the three known polymorphs the 8/1/4 composition in alkali-phosphidogermanates. All polymorphs are degraded from the aristotype CaF_2. The new polymorph of Na_8GeP_4 is obtained by two *klassengleiche* transitions of which the latter introduces a doubling of the cell parameters.

In conclusion, the measurements reveal a range of two orders of magnitude between the electronic conductivities of the mixed compound and the phase pure $Na_{10}Ge_2P_6$ compound. Therefore, it can be concluded that Na_8GeP_4 shows purely electronic conductivity in the upper range of 10^{-3} S/cm^{-1} at room temperature.

The electronic property calculations were performed using quantum chemical methods at a DFT-PBE0/TZVP level of theory for all basis sets. The optimized structures of Na_8GeP_4 are in line with the experimental crystal structures and the deviation of the cell parameter are smaller than 1.35 %. The compound has an indirect band gap with a width of 1.9 eV (Figure 5). The direct band gap at Γ-point is only slightly larger, about 0.01 eV, thus it can be assumed that the compound has a pseudo-direct band gap. The valence bands show only a low dispersion, which could hint that the electrons are rather localized. The density of states (DOS) further shows that the top valence bands are centred around the eight P atoms with small contributions of Ge. In the lower conduction bands the contributions of Ge and P are equal, except for bands between 3–5 eV, which have more P atom contribution (Figure 5). Over the whole calculated energy range, the contribution of Na atoms seems large, however this is an artifact of the chosen basis set, which results in more possible states that are reflected in the DOS. In general, alkali metal atoms are described by a SVP basis set to decrease the cost of the calculations while maintaining accuracy. In our case a Na TZVP basis set was chosen to get a more accurate value for the band gap, since the calculations with a SVP basis set resulted in a rather large band gap. Considering a systematic error of overestimating the band gap of semiconducting materials up to +0.5 eV when using a PBE0 level of theory, the conductivity measurements hint a conductivity in the range of elemental Si, which has a band gap of about 1.2 eV, thus the band gap should be much smaller than the calculated 3.0 eV for a Na SVP basis set.[27] Since more than 50 % of the atoms in the unit cell are Na, we recalculated the band structure and DOS using a more accurate TZVP basis set for Na, resulting in an identical shape of the bands and DOS of Ge and P but much smaller band gap. This resulted in a gap of 1.9 eV, which is more in line with the conductivity measurement.

The crystal orbital overlap population (COOP) shows Ge and P bonding states just below the Fermi Level (Figure 6). Since there is a considerable higher high density of states in the same energy region, those extra states of the valence band can be assigned with non-bonding character expressing the various lone pairs located at the P atoms. This is in line with the high PDOS arising from P atoms as shown in Figure S12 (Supporting Information). At around −2.5 eV the number of bonding interactions increases. In combination with a simultaneous high PDOS of Ge and P atoms, the COOP curves are in agreement with covalent Ge–P interactions. As expected, for the conduction bands the COOP shows Ge–P anti-bonding interactions.

Conclusions

Na_8GeP_4 represents a new sodium rich phosphidotetrelate and the first representative in the system of sodium phosphidotetrelates that crystallizes with isolated $[GeP_4]^{8-}$ tetrahedra as structural motif. As it shows great similarities to the lithium-containing derivatives, that show high lithium ion mobility, it seemed to be a very interesting candidate for investigating the sodium ion conduction. Comparing Na_8GeP_4 to lithium phosphidotetrelates of the same stoichiometry, they share the same structural motif, however exhibit a different arrangement of the TtP_4 (Tt = Si, Ge, Sn) tetrahedra. Na_8GeP_4 crystallizes in the space group $Fd\bar{3}m$ (no. 227) which traces back to the same CaF_2 aristotype as α- and β-Li_8GeP_4 but does not show a direct symmetry relationship to either of these two. Nevertheless, it shares many structural aspects such as for example a *ccp* of phosphorous atoms or an ordering of the tetrel atoms and alkali ions in the voids of the packing resulting in overall 87,5 % occupation of tetrahedral

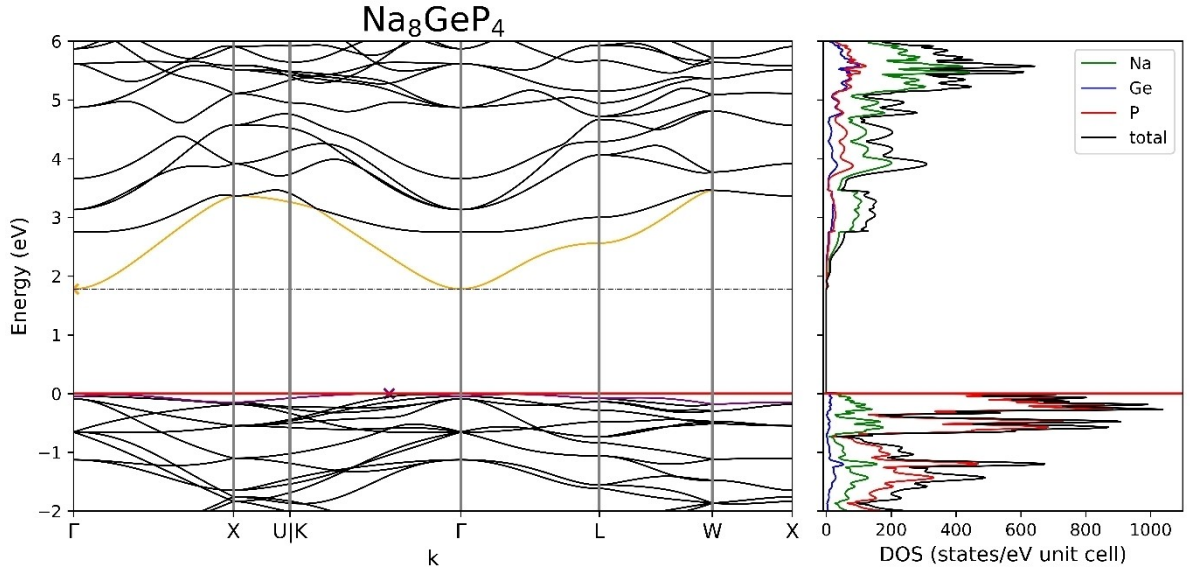

Figure 5. Band structure and density of states of Na_8GeP_4.

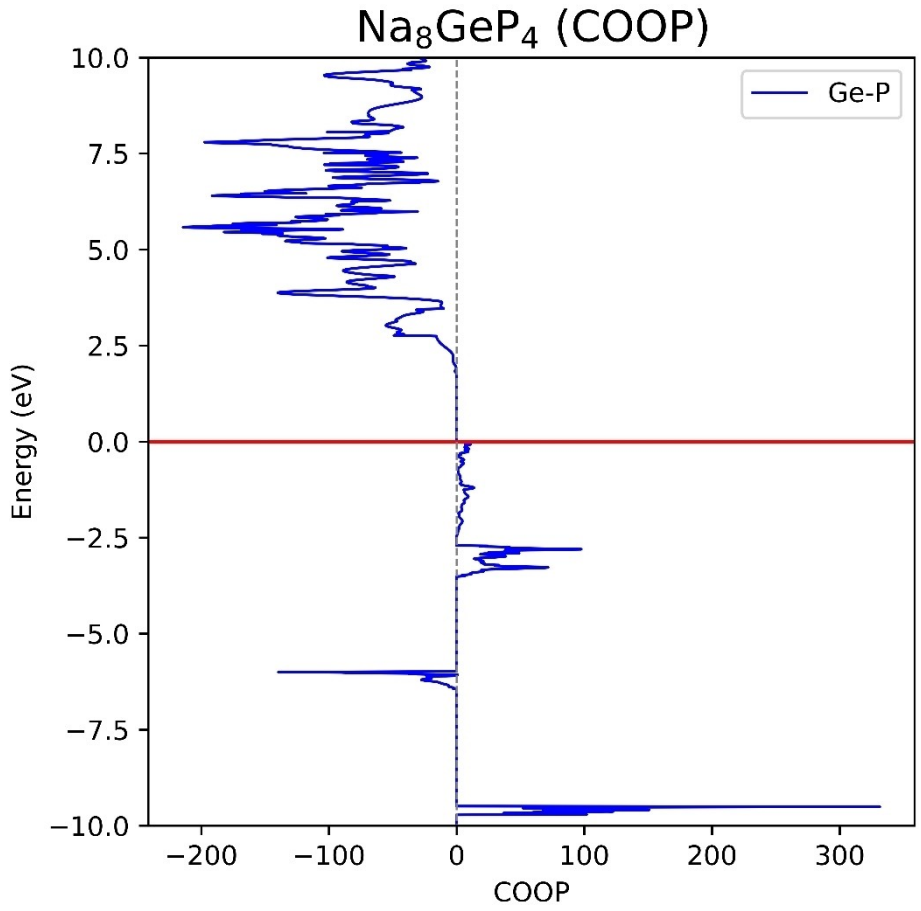

Figure 6. Crystal orbital overlap population of Ge and P. The red horizontal line marks the Fermi-Level, bonding interactions show positive values regarding the x-axis, anti-bonding interactions negative values.

voids and 50 % occupation of octahedral voids. Investigation of the electronic structure revealed that Na_8GeP_4 exhibits solely electronic conductivity and has a considerable band gap as confirmed by PEIS and DC measurements as well as DFT calculations, respectively.

Supporting information

The Supporting information contains Details on Experimental-powder-XRD Measurements as well as additional crystallographic data. Furthermore, it contains experimental data on DSC and PEIS Measurements as well as details on the quantum chemical calculations. It also contains information on the symmetry relationship of Na_8GeP_4.

Acknowledgements

The authors are very grateful to Dominik Dankert for the Raman Measurements and fruitful discussion on the obtained data. Open Access funding enabled and organized by Projekt DEAL.

Conflict of Interest

The authors declare no conflict of interest.

Data Availability Statement

The data that support the findings of this study are available in the supplementary material of this article.

[1] J. B. Goodenough, K.-S. Park, *J. Am. Chem. Soc.* **2013**, *135*, 1167–1176.
[2] a) H. Pan, Y.-S. Hu, L. Chen, *Energy Environ. Sci.* **2013**, *6*, 2338–2360; b) S. Ohno, W. G. Zeier, *Nat. Energy* **2022**, *7*, 686–687; c) M. D. Slater, D. Kim, E. Lee, C. S. Johnson, *Adv. Funct. Mater.* **2013**, *23*, 947–958.
[3] P. Barpanda, G. Oyama, S.-I. Nishimura, S.-C. Chung, A. Yamada, *Nat. Commun.* **2014**, *5*, 4358.
[4] B. Shao, Y. Huang, F. Han, *Adv. Energy Mater.* **2023**, *13*, 2204098.
[5] J. B. Goodenough, H. Y. P. Hong, J. A. Kafalas, *Mater. Res. Bull.* **1976**, *11*, 203–220.
[6] a) A. Hayashi, K. Noi, A. Sakuda, M. Tatsumisago, *Nat. Commun.* **2012**, *3*, 856; b) T. Krauskopf, S. P. Culver, W. G. Zeier, *Inorg. Chem.* **2018**, *57*, 4739–4744.
[7] M. Duchardt, U. Ruschewitz, S. Adams, S. Dehnen, B. Roling, *Angew. Chem. Int. Ed.* **2018**, *57*, 1351–1355.
[8] A. Haffner, T. Bräuniger, D. Johrendt, *Angew. Chem. Int. Ed.* **2016**, *55*, 13585–13588.
[9] a) L. Toffoletti, H. Kirchhain, J. Landesfeind, W. Klein, L. van Wüllen, H. A. Gasteiger, T. F. Fässler, *Chem. Eur. J.* **2016**, *22*, 17635–17645; b) H. Eickhoff, S. Strangmüller, W. Klein, H. Kirchhain, C. Dietrich, W. G. Zeier, L. van Wüllen, T. F. Fässler, *Chem. Mater.* **2018**, *30*, 6440–6448; c) S. Strangmüller, H. Eickhoff, W. Klein, G. Raudaschl-Sieber, H. Kirchhain, T. Kutsch, V. Baran, A. Senyshyn, L. van Wüllen, H. A. Gasteiger, T. F. Fässler, *J. Mater. Chem. A* **2021**, *9*, 15254–15268.
[10] a) S. Strangmüller, H. Eickhoff, D. Müller, W. Klein, G. Raudaschl-Sieber, H. Kirchhain, C. Sedlmeier, V. Baran, A. Senyshyn, V. L. Deringer, L. van Wüllen, H. A. Gasteiger, T. F. Fässler, *J. Am. Chem. Soc.* **2019**, *141*, 14200–14209; b) S. Strangmüller, H. Eickhoff, G. Raudaschl-Sieber, H. Kirchhain, C. Sedlmeier, L. van Wüllen, H. A. Gasteiger, T. F. Fässler, *Chem. Mater.* **2020**, *32*, 6925–6934.
[11] a) T. M. F. Restle, C. Sedlmeier, H. Kirchhain, W. Klein, G. Raudaschl-Sieber, V. L. Deringer, L. van Wüllen, H. A. Gasteiger, T. F. Fässler, *Angew. Chem. Int. Ed.* **2020**, *59*, 5665–5674; b) T. M. F. Restle, C. Sedlmeier, H. Kirchhain, W. Klein, G. Raudaschl-Sieber, L. van Wüllen, T. F. Fässler, *Chem. Mater.* **2021**, *33*, 2957–2966; c) T. M. F. Restle, S. Strangmüller, V. Baran, A. Senyshyn, H. Kirchhain, W. Klein, S. Merk, D. Müller, T. Kutsch, L. van Wüllen, T. F. Fässler, *Adv. Funct. Mater.* **2022**, *32*, 2112377.
[12] a) A. Haffner, A.-K. Hatz, O. E. O. Zeman, C. Hoch, B. V. Lotsch, D. Johrendt, *Angew. Chem. Int. Ed.* **2021**, *60*, 13641–13646; b) A. Haffner, A.-K. Hatz, I. Moudrakovski, B. V. Lotsch, D. Johrendt, *Angew. Chem. Int. Ed. Engl.* **2018**, *57*, 6155–6160.
[13] a) H. Eickhoff, V. Hlukhyy, T. F. Fässler, *Z. Anorg. Allg. Chem.* **2020**, *646*, 1834–1838; b) K. Feng, W. Yin, R. He, Z. Lin, S. Jin, J. Yao, P. Fu, Y. Wu, *Dalton Trans.* **2012**, *41*, 484–489.
[14] B. Eisenmann, M. Somer, *Z. Naturforsch. B* **1985**, *40*, 886–890.
[15] STOE & Cie GmbH, Darmstadt, Germany, **2011**.
[16] Institute Laue-Langevin, Grenoble, France, **2020**.
[17] B. Eisenmann, J. Klein, *Z. Naturforsch. B* **1988**, *43*, 1156.
[18] Netzsch-Gerätebau GmbH, Selb, **2006**.
[19] Renishaw plc, Gloucestshire, **2002**.
[20] a) R. Dovesi, V. R. Saunders, C. Roetti, R. Orlando, C. M. Zicovich-Wilson, F. Pascale, B. Civalleri, K. Doll, N. M. Harrison, I. J. Bush, P. D'Arco, M. Llunell, M. Causà, Y. Noël, L. Maschio, A. Erba, M. Rerat, S. Casassa, *CRYSTAL17 User's Manual*, University of Torino, **2017**; b) R. Dovesi, A. Erba, R. Orlando, C. M. Zicovich-Wilson, B. Civalleri, L. Maschio, M. Rerat, S. Casassa, J. Baima, S. Salustro, B. Kirtman., *WIREs Comput Mol Sci.* **2018**, 8: e1360.
[21] a) J. P. Perdew, K. Burke, M. Ernzerhof, *Phys. Rev. Lett.* **1996**, *77*, 3865–3868; b) C. Adamo, V. Barone, *J. Chem. Phys.* **1999**, *110*, 6158–6170.
[22] a) F. Weigend, R. Ahlrichs, *Phys. Chem. Chem. Phys.* **2005**, *7*, 3297–3305; b) F. Weigend, M. Häser, H. Patzelt, R. Ahlrichs, *Chem. Phys. Lett.* **1998**, *294*, 143–152.
[23] Y. Hinuma, G. Pizzi, Y. Kumagai, F. Oba, I. Tanaka, *Comput. Mater. Sci.* **2017**, *128*, 140–184.
[24] T. J. Team, **2019**, http://www.jmol.org/.
[25] B. Eisenmann, J. Klein, *Z. Naturforsch. B* **1988**, *43*, 69.
[26] a) H. Eickhoff, C. Dietrich, W. Klein, W. G. Zeier, T. F. Fässler, *Z. Anorg. Allg. Chem.* **2021**, *647*, 28–33; b) G. Nazri, *Solid State Ionics* **1989**, *34*, 97–102.
[27] B. Civalleri, D. Presti, R. Dovesi, A. Savin, in *Chemical Modelling: Applications and Theory Volume 9, Vol. 9*, The Royal Society of Chemistry, **2012**, pp. 168–185.

Manuscript received: July 27, 2023
Revised manuscript received: August 29, 2023
Accepted manuscript online: August 31, 2023

